26th International Congress of Mechanical Engineering
COBEM 2021
November 22-26, 2021, Virtual Congress, Brazil

COB-2021-2349
FLUTTER STABILITY ANALYSIS OF A PLATE-LIKE WING SYSTEM IN THE PRESENCE OF PARAMETRIC UNCERTAINTY

Marcelo Araújo Delgado Filho
Antônio Marcos Gonçalves de Lima
Gutembergy Ferreira Diniz
Faculdade de Engenharia Mecânica, Universidade Federal de Uberlândia Av. João Naves de Ávila 2121, Campus Santa Mônica, 384000-902, Uberlândia/Minas Gerais, Brasil
marcelo.delgado@ufu.br, amglima@ufu.br, gutembergy_ferreira@hotmail.com

Abstract. *When conducting stability analysis of aeroelastic systems, it is relevant to consider possible sources of uncertainty, as they may considerably modify its dynamic behavior. In structural engineering, randomness is present in the geometrical and physical parameters of the system and even in the mathematical model. Regarding a plate-like wing arrangement, thickness variation has considerable potential to change the aeroelastic response. Concomitantly, flutter is one of the most fundamental aeroelastic instabilities. Therefore, this work has attempted to study the effect of thickness variation on the flutter velocity of a cantilevered thin plate. Due to the bi-dimensional nature of the structure, the random thickness is represented by the Karhunen-Loève expansion as a Gaussian random field. The doublet lattice method and the pk method yield the unsteady aerodynamic load and the flutter velocity, respectively. By propagating uncertainty into the equation of motion through Monte Carlo simulation, it is possible to represent the flutter phenomenon more realistically when compared with the deterministic approach. The relevance of including uncertainty in such aeroelastic systems is, thus, demonstrated.*

Keywords: *flutter, uncertainty quantification, parametric uncertainty, plate-like wing model.*

1. INTRODUCTION

Aeronautical structures are inherently light, causing them to considerably deform when subjected to aerodynamic loads, originating a quite complex behavior in which deformation and load are interdependent (Garrick and Reed, 1981). This interaction may lead to dangerous aeroelastic phenomena. One of the most important aeroelastic instabilities is flutter, a self-excited vibration caused by an unfavorable coupling between two or more vibration modes (Wright and Cooper, 2015). At a particular critical velocity, flutter is a condition in which, given a slight increase in flow velocity, one of the modes becomes negatively damped, causing the structure to extract energy from the surrounding air stream and oscillate, usually with high amplitude (Fung, 1993; Wright and Cooper, 2015). Given the possibility of structural failure due to these unstable vibrations, flutter can not be allowed to occur within the aircraft's flight envelope and must be accounted for and accurately predicted during the design phase.

Although there are well-established methodologies for the critical flutter velocity computation, the usual approach does not consider variations of the system parameters. Yet, these variations do exist and may highly modify the system response. Manufacturing and measurement imprecision, inconstant material properties, environmental changes, and even the proposed mathematical model itself are some of the sources of uncertainty in engineering applications. Given that these sources can not be eliminated, it is necessary to investigate their influence to achieve safe and efficient aircraft, which has been a very active research topic (Dai and Yang, 2014).

Regarding parametric sources of uncertainty in wing configurations, it has been shown (Kurdi *et al.*, 2007; Khodaparast *et al.*, 2010) that thickness, among other geometric dimensions, can considerably influence the aeroelastic response, even for deviations as small as 5 %. Since a wing is predominantly a bi-dimensional structure, it would be relevant to consider the spatial variability of the random thickness along with each of these dimensions as a random field. One way of accomplishing this is by employing the Karhunen-Loève (KL) decomposition, as proposed here. Hence, the objective of this work was to develop a stochastic aeroelastic model of a rectangular wing, represented by a thin plate, to quantify the impact of the uncertain thickness on the flutter velocity.

2. AEROELASTIC MODELING

The aeroelastic system considered in this work is the thin cantilevered plate studied by Conyers *et al.* (2010). Thus a plate-like wing configuration is considered, as in Fig. 1. The plate dimensions are also displayed. In the present case, the thickness will be a random variable with Gaussian distribution and a coefficient of variation, $COV = \sigma/\mu$, of 0.05. The remaining parameters are set constant, including material-related ones. It is worth mentioning that the plate is composed of polycarbonate, whose physical properties are in Tab. 1.

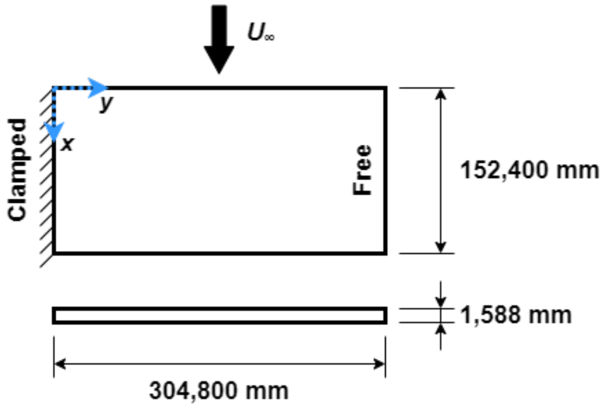

Figure 1. Cantilevered plate studied by Conyers *et al.* (2010).

Table 1. Material properties of the cantilevered plate studied by Conyers *et al.* (2010).

Property	**Value**
Density (ρ)	1217 kg/m^3
Young's Modulus (E)	2.4 GPa
Poisson's ratio (ν)	0.33

The system's equation of motion is necessary to perform the stability analysis. With this objective, finite elements are used to describe the inertial and stiffness characteristics of the structure, as discussed in section 2.1. The thickness in the elementary matrices will be represented as a bi-dimensional random field by the KL expansion. Next, in section 2.2, the doublet lattice method (DLM) is used to model the unsteady aerodynamic load, and the aeroelastic equation of motion is obtained in section 2.3. The pk method is then employed to compute the resulting flutter velocity in section 2.4.

One of the most straightforward ways to propagate uncertainty into the mathematical model is the Monte Carlo method. This technique generates a random sample according to a given probability density function and then computes the outcome for each sample through the mathematical model. Although usually associated with high computational costs, Monte Carlo may still be a viable methodology for the considered system, especially if modal representation is used and the aerodynamic forcing terms are approximated from discrete previously calculated points (Beran *et al.*, 2017).

2.1 Stochastic Structural Model

The dynamic behavior of the system is modeled by the finite element method (FEM). If the structural damping is disregarded, the system's dynamical behavior is given by Eq. (1):

$$[M]\{\ddot{\delta}\} + [K]\{\delta\} = \{F(t)\}, \tag{1}$$

where $[M]$ and $[K]$ are computed from their corresponding elementary matrices $[M_i]$ and $[K_i]$, by expanding them in global coordinates using the transformation matrices $[\gamma_i]$, as displayed in Eq. (2):

$$[M] = \sum_{i=1}^{ne} [\gamma_i]^{\mathrm{T}} [M_i] [\gamma_i], \tag{2}$$

and Eq. (3):

$$[K] = \sum_{i=1}^{ne} [\gamma_i]^{\mathrm{T}} [K_i] [\gamma_i]. \tag{3}$$

As in Fig. 2, each plate element has four nodes (k, l, m, n) and three degrees of freedom per node, being two of rotation (θ_x, θ_y) and one of displacement (w). The elementary dimensions are a and b. Employing the Kirchhoff-Love plate theory, the element is considered thin, and a plane stress state develops. Thus, the deformation vector is in the form of Eq. (4):

$$\{\varepsilon\} = -z\left\{ \frac{\partial^2 w}{\partial x^2} \quad \frac{\partial^2 w}{\partial y^2} \quad 2\frac{\partial^2 w}{\partial x \partial y} \right\}^{\mathrm{T}}, \tag{4}$$

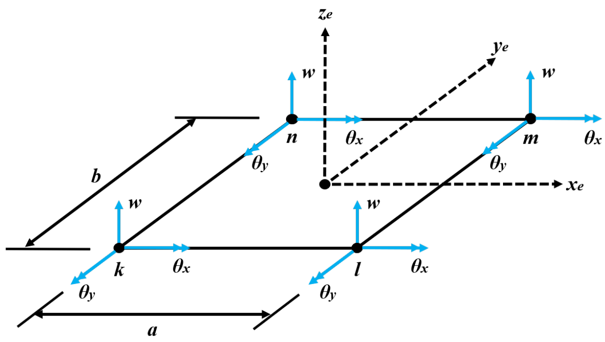

Figure 2. Plate Finite Element.

where w is approximated by the shape functions $N(x,y)$ and nodal displacements of the ith element, as in Eq. (5):

$$w\left(x,y\right)=N\left(x,y\right)\left\{\delta_i\right\}. \tag{5}$$

It is worth mentioning that a two-dimensional third-order polynomial is used for the approximation.

If a linear elastic regime is assumed, the elementary stiffness matrix may be obtained from the potential strain energy of the finite element as:

$$[K_i]=\iint\limits_A \frac{h^3}{12}E[B]^{\mathrm{T}}\left[A\right]\left[B\right]dA \tag{6}$$

in which:

$$[A]=\frac{1}{1-\nu^2}\begin{bmatrix}1 & \nu & 0\\ \nu & 1 & 0\\ 0 & 0 & \frac{1-\nu}{2}\end{bmatrix}, \tag{7}$$

and $[B]$ is defined by Eq. (8):

$$[B]=\left\{\frac{\partial^2 N}{\partial x^2} \quad \frac{\partial^2 N}{\partial y^2} \quad 2\frac{\partial^2 N}{\partial x \partial y}\right\}^{\mathrm{T}}. \tag{8}$$

Similarly, the elementary mass matrix $[M_i]$ can be obtained from the kinetic energy of the finite element, as written in Eq. (9):

$$[M_i]=\iint\limits_A \rho h N(x,y)^{\mathrm{T}}N\left(x,y\right)dA. \tag{9}$$

Equation (6) and Eq. (9) for $[M_i]$ and $[K_i]$, respectively, are dependent upon the thickness h, that will be considered a Gaussian random process. The Karhunen-Loève (KL) expansion is used to represent this process. Hence, h is composed by the sum of its mean value, $\bar{h}$, constant since the process is stationary, and a stochastic contribution in the form of a truncated series of order n, as in Eq. (10):

$$h\left(x,y,\varepsilon\right)=\bar{h}+\sum_{r=1}^{n}\sqrt{\lambda_r}f_r\left(x,y\right)\xi_r\left(\varepsilon\right). \tag{10}$$

The terms $\xi_r(\varepsilon)$ are zero-mean Gaussian random variables, the samples, while $\lambda_r=\lambda_i\lambda_j$ are the eigenvalues and $f_r\left(x,y\right)=f_i\left(x\right)f_j\left(y\right)$ the eigenfunctions of the eigenvalue problem related to the exponential covariance function of the process, as proposed by Ghanem and Spanos (1991). According to the authors, the eigenfunctions are found analytically to be defined by Eq. (11), for odd values of r, and by Eq. (12), for even values of r:

$$f_i\left(x\right)=\frac{\cos(\omega_i x)}{\sqrt{\tau_x+\frac{\mathrm{sen}(2\omega_i\tau_x)}{2\omega_i}}},\ f_j\left(y\right)=\frac{\cos(\omega_j y)}{\sqrt{\tau_y+\frac{\mathrm{sen}(2\omega_j\tau_y)}{2\omega_j}}} \tag{11}$$

$$f_i\left(x\right)=\frac{\mathrm{sen}(\omega_i x)}{\sqrt{\tau_x-\frac{\mathrm{sen}(2\omega_i\tau_x)}{2\omega_i}}},\ f_j\left(y\right)=\frac{\mathrm{sen}(\omega_j y)}{\sqrt{\tau_y-\frac{\mathrm{sen}(2\omega_j\tau_y)}{2\omega_j}}}. \tag{12}$$

The solution for the eigenvalues is written in Eq. (13):

$$\lambda_i = \frac{2}{\left(\omega_i{}^2 + \left(\frac{1}{L_x}\right)^2\right) L_x}, \ \lambda_j = \frac{2}{\left(\omega_j{}^2 + \left(\frac{1}{L_y}\right)^2\right) L_y}. \tag{13}$$

The terms ω_i and ω_j are the solutions of transcendental equations, which also vary for odd and even values of r. In the first situation, these solutions are in the form of Eq. (14):

$$\frac{1}{L_x} - \omega_i \tan(\omega_i \tau_x) = 0, \ \frac{1}{L_y} - \omega_j \tan(\omega_j \tau_y) = 0. \tag{14}$$

In the second situation, for r even, the solutions take the form of Eq. (15):

$$\omega_i + \frac{1}{L_x} \tan(\omega_i \tau_x) = 0, \ \omega_j + \frac{1}{L_y} \tan(\omega_j \tau_y) = 0. \tag{15}$$

It is necessary to mention that L_x and L_y are the correlation lengths in the x and y directions, respectively, considered equal to the elementary dimensions in their correspondent directions, a and b. Also, $\tau_x = a/2$ and $\tau_y = b/2$ define the limits of domain $D = [-\tau_x, \tau_x] \cdot [-\tau_y, \tau_y]$ where the random process is considered.

2.2 Aerodynamic Loading

Once the left-hand side of Eq. (1) has been obtained considering the effect of the random thickness, it is necessary to compute the unsteady aerodynamic load acting on the structure. The Doublet Lattice Method (DLM), proposed by Albano and Rodden (1969) to model the lift generated by a non-stationary flow, is used for this task. It represents the lifting surface by a set of panels arranged in columns parallel to the flow, as displayed in Fig. 3. Each panel has a line of potential acceleration doublets, positioned at $1/4$ of the panel chord, c. The flow induced by the doublet line is an elementary solution for the aerodynamic potential, linearized around a subsonic and uniform flow along the x-axis. This solution and the boundary conditions for the induced velocity at the control point, located at $3/4$ of c, are used to obtain the pressure distribution over the wing.

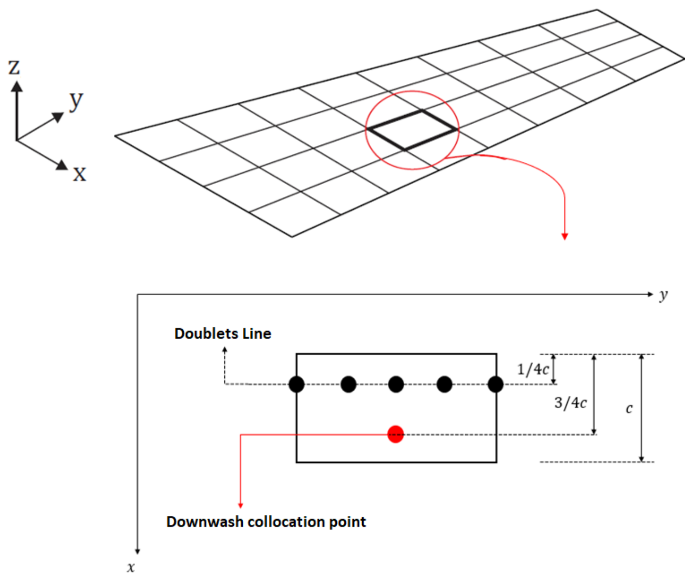

Figure 3. Representation of a generic lifting surface by the DLM.

The complete mathematical development of DLM is far too extensive to be presented here. Briefly, the method may be summarized by Eq. (16):

$$\{\Delta c_p\} = [AIC]\{w_N\}, \tag{16}$$

which states that the pressure coefficients at each control point are computed from the aerodynamic influence coefficients matrix, $[AIC]$, related to the pressure difference due to the influence of one panel on another, and the vector $\{w_N\}$ of induced velocities at the control points. These are named downwash velocities and normalized by the flow velocity U_∞. They are computed by satisfying the boundary conditions of the flow, which state that there are no components normal to the surface, and the flow is tangent to it (Silva, 2018). For a single panel, these conditions are expressed mathematically by Eq. (17):

$$w_N = \frac{ik}{b}h + \frac{\partial h}{\partial x}, \tag{17}$$

where i is the imaginary unit, b is the semi-chord of the wing, k is the reduced frequency, and h is the modal displacement of the structure at the downwash collocation point.

It is more convenient to write Eq. (17) in matrix form to represent all panels:

$$\{w_N\} = ([D_R] + ik\,[D_I])\,\{h\}^{\mathrm{T}}. \tag{18}$$

In Eq. (18), $[D_R]$ and $[D_I]$ are differentiation matrices associated with the magnitude of h and the amplitude of their variations with x, respectively.

Finally, the loading vector $\{F_a\}$, containing the forces at each control point, may be obtained from Eq. (16) by multiplying the pressure coefficients by the dynamic pressure q_∞ and the matrix $[S]$ with the areas of each panel:

$$\{F_a\} = q_\infty\,[S]\,[AIC]\,\{w_N\}. \tag{19}$$

2.3 Aeroelastic Model

The point of connection between the structural and aerodynamic models is the modal displacement h. Using an interpolation matrix $[T_{as}]$, the modal displacements vector $\{h\}$ is computed from the displacement $\{\delta\}$ at the nodes of the finite elements:

$$\{h\}^{\mathrm{T}} = [T_{as}]\,\{\delta\}\,. \tag{20}$$

Thus, it is worth mentioning that, in this study, the plate's finite elements are coincident with the panels of the DLM, as in Fig. 4. From this figure, it is noticeable that to insert the aerodynamic load into the finite element model is necessary to interpolate once more using splines. Therefore, the force vector at the nodes of the finite elements is given by Eq. (21):

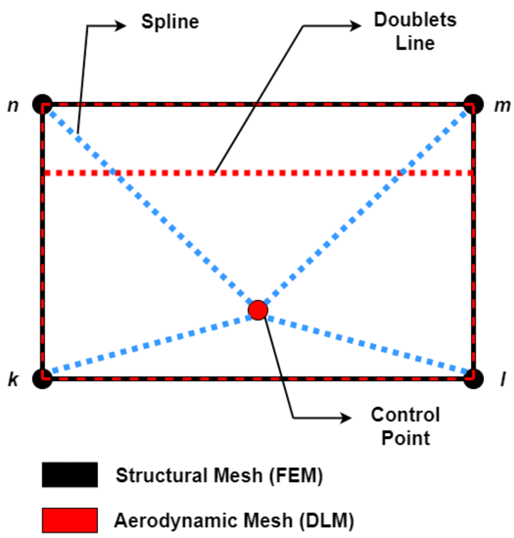

Figure 4. Structural and aerodynamic meshes on a plate element.

$$\{F_s\} = [T_{as}]^{\mathrm{T}}\,\{F_a\}. \tag{21}$$

Additionally, if the load is written as a function of the modal coordinates, $\{\delta\} = [\Phi]\,\{q\}$, the load vector becomes:

$$\{F_q\} = q_\infty\,[Q\,(k)]\,\{q\}\,, \tag{22}$$

where $[Q\,(k)]$ is the generalized aerodynamic matrix (GAM), defined as:

$$[Q\,(k)] = [\Phi]^{\mathrm{T}}[T_{as}]^{\mathrm{T}}\,[S]\,[AIC]\,([D_R] + ik\,[D_I])\,[T_{as}]\,[\Phi]. \tag{23}$$

The motivation to describe the equation of motion in modal coordinates is to reduce the computation costs by considering only the first modes of the modal matrix $[\Phi]$, therefore reducing the problem order. Writing Eq. (1) also in modal coordinates and combining with Eq. (23), the system's equation of motion is obtained as:

$$[M_q]\,\{\ddot{q}\} + [K_q]\,\{q\} = q_\infty\,[Q\,(k)]\,\{q\}. \tag{24}$$

2.4 Flutter Computation

The critical flutter velocity is computed by observing the behavior of the damping associated with each vibration mode. If a mode becomes unstable at a given velocity, flutter is to happen. Within this regard, the following eigenvalue problem associated with Eq. (24) is proposed:

$$\left(p^2 [M_q] + [K_q] - q_\infty [Q(k)]\right) \{q\} = 0, \tag{25}$$

where the eigenvalue p is related to damping g by Eq. (26):

$$p = \omega \left(\frac{g}{2} \pm i\right). \tag{26}$$

However, considering that $[Q(k)]$ depends upon the reduced frequency k, there is one difficulty in solving Eq. (25), as k is by its very definition related to the circular frequency ω:

$$k = \frac{\omega b}{U_\infty}, \tag{27}$$

which is the imaginary part of p as in Eq. (26). Therefore, there is one equation and two unknowns. The well-known pk method is used to deal with this situation. It consists of solving Eq. (25) iteratively for each mode and each airstream velocity until convergence is obtained. Hence, it is possible to construct the curves of damping versus velocity, that is, the v-g diagram, and thus determine the critical flutter velocity, as intended.

It is relevant to highlight that to reduce the cost associated with the iterative procedure, $[Q(k)]$ is computed through interpolation of discrete previously obtained $[Q(k)]$ values for a set of reduced frequencies k.

3. RESULTS

The results are divided into two sections. First, the proposed numeric model is compared with experimental results from the literature for the nominal system configuration with no uncertainty. Then in the following section, the thickness is considered random, and its effect on the flutter velocity is quantified.

3.1 Nominal System

For the nominal configuration, the curves of damping and natural frequency as a function of the flow velocity are given, in Fig. 5 and Fig. 6, for the first four modes. It is seen that the second mode is unstable, and the flutter velocity is obtained by observing the point where the associated damping becomes positive. Thus the flutter velocity is 19.0 m/s. This result represents a difference of 5.24 % from the experimental value obtained by Conyers *et al.* (2010) and may be considered a reasonable approximation of the real aeroelastic behavior of the system.

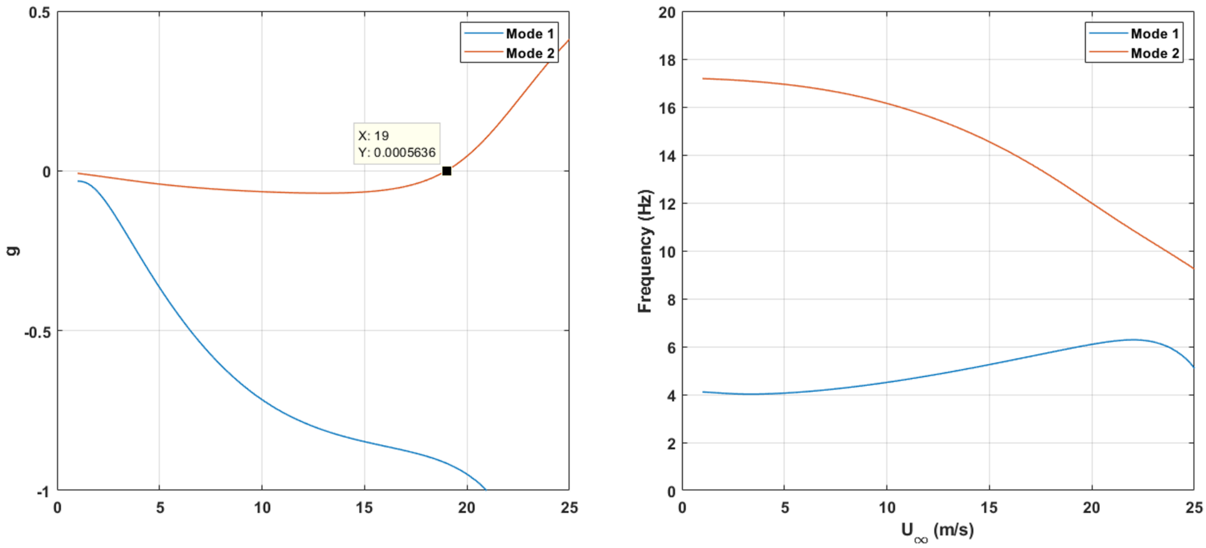

Figure 5. v-g (right) and v-f (left) diagrams for the first two modes.

It is also possible to note that the frequencies of modes 1 and 2 tend to coalesce, which does not happen due to the aerodynamic damping. This behavior suggests that the coupling between these two modes. Furthermore, modes 3 and 4 remain stable and play no role in the instability development, as can be seen. Thus it is a case of binary flutter.

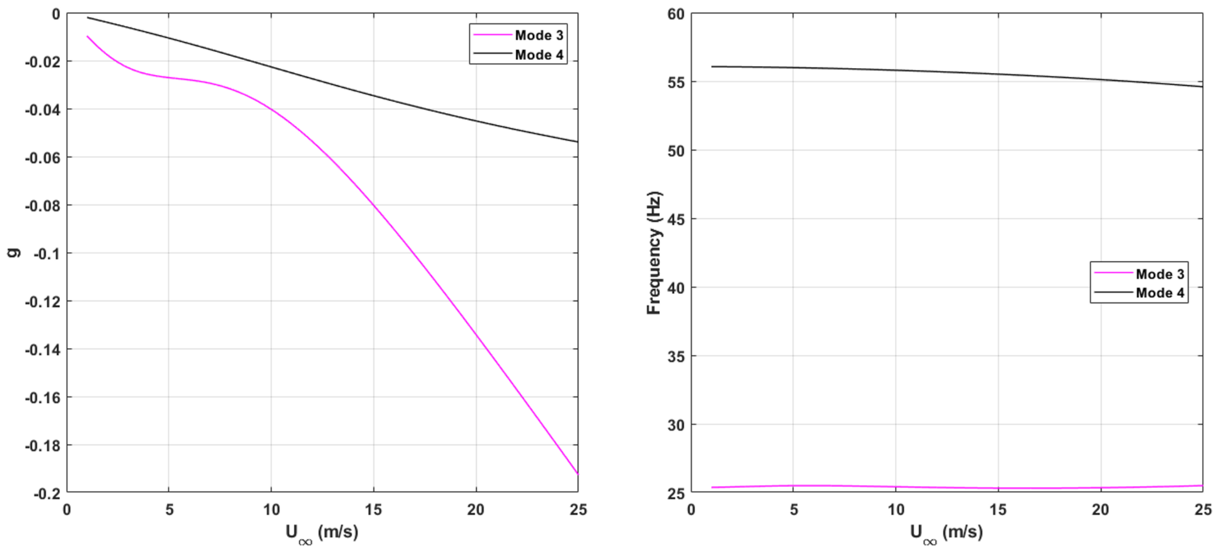

Figure 6. v-g (right) and v-f (left) diagrams for the first modes 3 and 4.

The analysis was restricted to the first four modes so that $[\Phi]$ also acts as a reduction basis. Therefore its size is limited and defined based on Fig. 7, where the convergence of the flutter velocity was obtained for the first four modes.

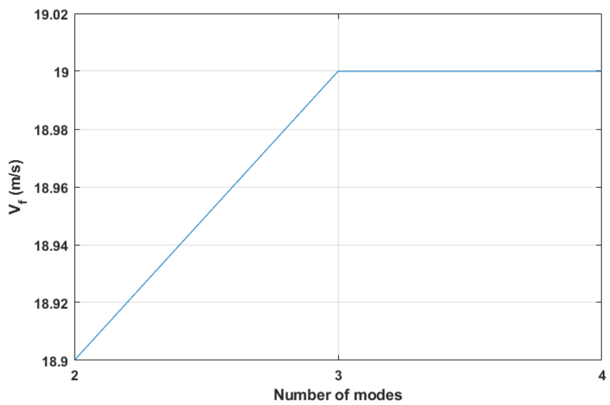

Figure 7. Convergence of the flutter velocity of the nominal system with the number of modes.

3.2 Stochastic System

For the stochastic configuration, it is necessary to analyze the convergence of two additional simulation parameters: the truncation order n of the KL expansion and the Monte Carlo simulation's sample number. The latter is determined from Fig. 8, where it can be seen that both eigenvalues tend to zero as the truncation order is increased. Hence, n is considered 5. The number of samples used was 1000 since the root mean square error (RMS) of the mean flutter velocity stabilizes for this value, as displayed in Fig. 9. This means that there is no further improvement of the result if more samples are generated.

Once all parameters were defined, it was possible to obtain the v-g and v-f envelopes corresponding to the first two modes, which are associated with the flutter instability. The results are shown in Fig. 10. It can be seen that before 15 m/s the uncertainty effect is negligible for the second mode. Then, at the proximity of the nominal flutter velocity, the curves start to separate, originating an envelope. For the first mode, the effect of the uncertainty is also small at the beginning, but, with the increase of the flow velocity, the curves show a continuous deviation from each other. The variation on the damping curves of the second mode will cause a variation in the flutter velocity. As can be seen, it ranges from 17.0 m/s to 21.1 m/s. As for the nominal case, the natural frequencies tend to coalesce.

To better visualize the impact of the considered uncertainty in the flutter velocity, its histogram is plotted in Fig. 11. As expected, the critical velocity distribution is Gaussian. It is also possible to note that the velocity is not significantly affected by the uncertainty in this case. Indeed, a COV of $5.00\,\%$ in the thickness generated a $3.79\,\%$ COV on the

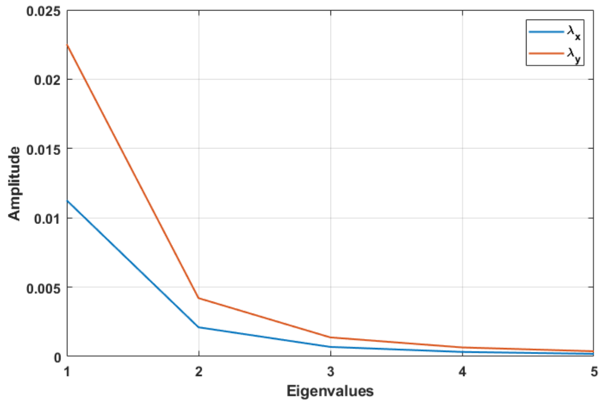

Figure 8. Eigenvalues of the KL expansion.

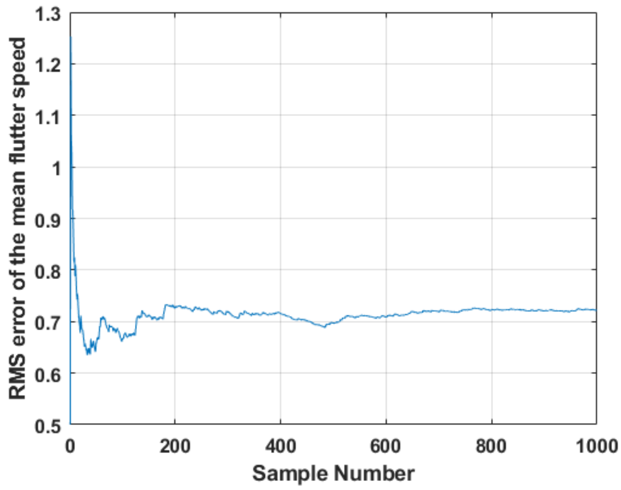

Figure 9. RMS error of the mean flutter velocity with the sample number.

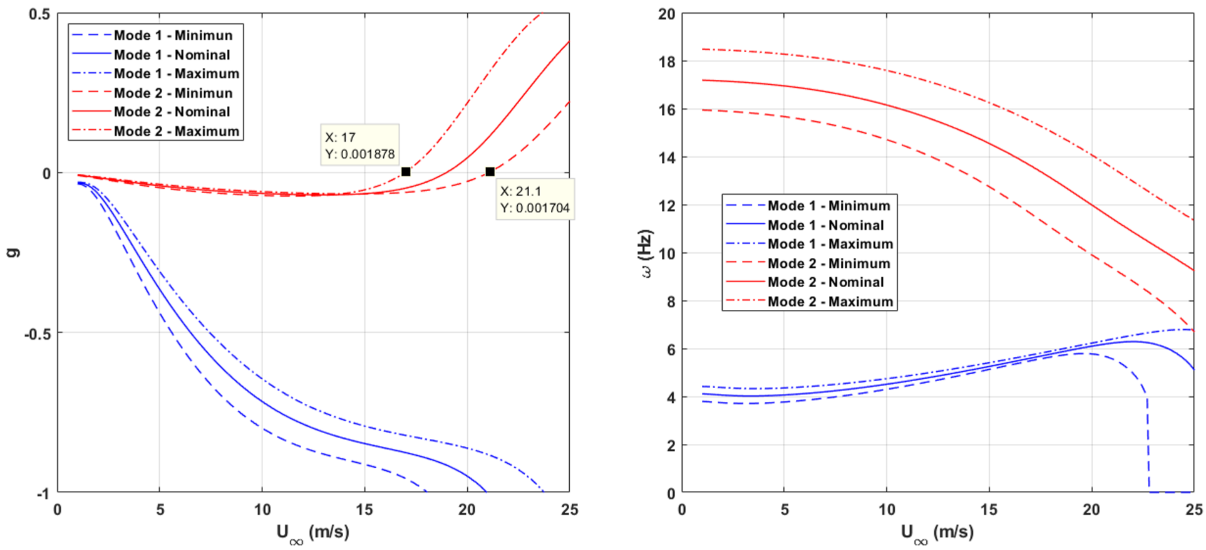

Figure 10. v-g and v-f envelopes for the first two modes.

flutter velocity, with a standard deviation of 0.72. Nevertheless, it is relevant to have a precise computation of the stability boundary, considering the dangerous nature of flutter.

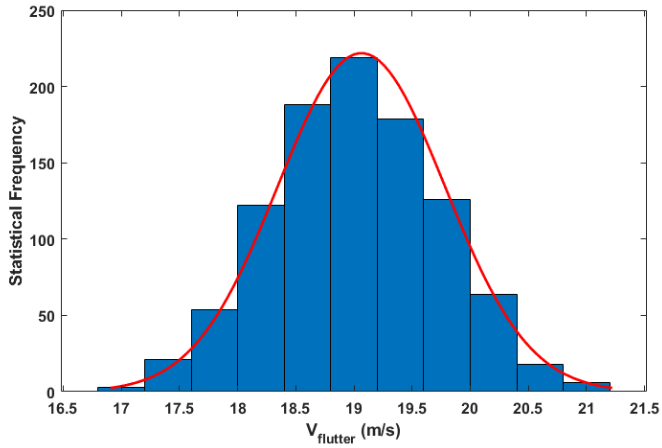

Figure 11. Histogram of the flutter velocity.

4. CONCLUSIONS

This study has attempted to quantify the effect of thickness variation on the critical flutter velocity of a plate-like wing system. The KL expansion was employed and combined with FEM to yield a structural stochastic model of the system that accounts for the spatial variability of the random thickness. Then the load was modeled by the DLM, and the aeroelastic equation of motion was obtained. Finally, the flutter velocity was computed by the pk method and uncertainty propagated through the Monte Carlo approach.

The proposed model was found consistent with the experimental results of the literature. Furthermore, the importance of considering potential sources of uncertainty to obtain a more realistic and precise prediction of the potentially dangerous flutter phenomenon was demonstrated, as it may happen before the expected nominal value.

5. ACKNOWLEDGMENTS

The authors are grateful to CNPq for the continued support to their research activities through the research grant 306138/2019-0 (A.M.G. de Lima). It is also important to express the acknowledgments to the CAPES and FAPEMIG to the research projects APQ-01865 and PPM-0058-18 (A.M.G. de Lima).

6. REFERENCES

Albano, E. and Rodden, W.P., 1969. "A doublet-lattice method for calculating lift distributions on oscillating surfaces in subsonic flows". *AIAA Journal*, Vol. 7, No. 2, pp. 279–285. doi:10.2514/3.5086. URL `https://doi.org/10.2514/3.5086`.

Beran, P., Stanford, B. and Schrock, C., 2017. "Uncertainty Quantification in Aeroelasticity". *Annual Review of Fluid Mechanics*, Vol. 49, No. 1, pp. 361–386. doi:10.1146/annurev-fluid-122414-034441.

Conyers, H.J., Dowell, E.H. and Hall, K.C., 2010. "Aeroelastic Studies of a Rectangular Wing with a Hole: Correlation of Theory and Experiment". In *Aerospace Systems Conference*. Los Angeles, p. 6.

Dai, Y. and Yang, C., 2014. "Methods and advances in the study of aeroelasticity with uncertainties". *Chinese Journal of Aeronautics*, Vol. 27, No. 3, pp. 461–474. doi:10.1016/j.cja.2014.04.016.

Fung, Y.C., 1993. *An Introduction to The Theory of Aeroelasticity*. Dover Publications, Inc.

Garrick, I.E. and Reed, W.H., 1981. "Historical development of aircraft flutter". *Journal of Aircraft*, Vol. 18, No. 11, pp. 897–912. ISSN 00218669. doi:10.2514/3.57579. URL `https://arc.aiaa.org/doi/abs/10.2514/3.57579`.

Ghanem, R.G. and Spanos, P.D., 1991. *Stochastic Finite Elements: A Spectral Approach*. Springer New York, New York, NY. doi:10.1007/978-1-4612-3094-6.

Khodaparast, H.H., Mottershead, J.E. and Badcock, K.J., 2010. "Propagation of structural uncertainty to linear aeroelastic stability". *Computers and Structures*, Vol. 88, No. 3-4, pp. 223–236. doi:10.1016/j.compstruc.2009.10.005.

Kurdi, M., Lindsley, N. and Beran, P., 2007. "Uncertainty quantification of the Goland+ Wing's flutter boundary". *AIAA Atmospheric Flight Mechanics Conference*, Vol. 1, No. August, pp. 104–123. doi:10.2514/6.2007-6309.

Silva, L.A., 2018. *Modelagem Aeroviscoelástica de Painéis Sanduíches Planos Via Método dos Painéis*. Dissetação de mestrado, Universidade Federal de Uberlândia.

Wright, J.R. and Cooper, J.E., 2015. *Introduction to Aircraft Aeroelasticity and Loads* . Wiley, 2nd edition.

7. RESPONSIBILITY NOTICE

The authors are solely responsible for the printed material included in this paper.